SUPPORTING MATERIALS

MOLECULAR AND MECHANICAL CAUSES OF MICROTUBULE CATASTROPHE AND AGING

Pavel Zakharov[1], Nikita Gudimchuk[2,3,4], Vladimir Voevodin[3], Alexander Tikhonravov[3], Fazoil I. Ataullakhanov[2,3,4] and Ekaterina L. Grishchuk[1]

[1]Department of Physiology, Perelman School of Medicine, University of Pennsylvania, Philadelphia, USA 19104
[2]Center for Theoretical Problems of Physicochemical Pharmacology, Russian Academy of Sciences, Moscow, Russia 119991
[3]Moscow State University, Moscow, Russia 119899
[4]Federal Research Center of Pediatric Hematology, Oncology and Immunology, Moscow Russia 117198

Appendix A. Calculating gradients of the total MT energy

The derivative of the total energy of the system with respect to independent variables $q^i_{k,n}$ is given by the following equation:

$$\frac{\partial U_{total}}{\partial q^i_{k,n}} = \frac{\partial v^{lat}_{k,n}}{\partial q^i_{k,n}} + \frac{\partial v^{inter}_{k,n}}{\partial q^i_{k,n}} + \frac{\partial v^{intra}_{k,n}}{\partial q^i_{k,n}} + \frac{\partial g^{bending}_{k,n}}{\partial q^i_{k,n}} \quad \text{(Eq. S1)}$$

It includes terms corresponding to the lateral interactions, inter and intra longitudinal interactions between tubulin subunits and the bending energy (see Eqs. 1-5 in *Materials and Methods*). To accelerate calculations we used explicit analytical expressions for all energy gradients:

$$\begin{cases} \frac{\partial v^{lat}_{k,n}}{\partial q^i_{k,n}} = \left(A_{lat} \cdot \frac{r^{lat}_{k,n}}{r_0^2} \cdot \exp\left(\frac{-r^{lat}_{k,n}}{r_o}\right) \cdot \left(2 - \frac{r^{lat}_{k,n}}{r_o}\right) + \frac{2 \cdot b_{lat} \cdot r^{lat}_{k,n}}{d \cdot r_o} \cdot \exp\left(\frac{-\left(r^{lat}_{k,n}\right)^2}{d \cdot r_o}\right) \right) \cdot \frac{\partial r^{lat}_{k,n}}{\partial q^i_{k,n}} \\ \frac{\partial v^{intra}_{k,n}}{\partial q_k} = k \cdot r_{k,n} \cdot \frac{\partial r_{k,n}}{\partial q^i_{k,n}} \\ \frac{\partial g^{bending}_{k,n}}{\partial q^i_{k,n}} = \frac{\partial g^{bending}_{k,n}}{\partial \chi_{k,n}} \cdot \frac{\partial \chi_{k,n}}{\partial q^i_{k,n}} = B \cdot \left(\chi_{k,n} - \chi_o\right) \cdot \frac{\partial \chi_{k,n}}{\partial q^i_{k,n}} \end{cases} \quad \text{(Eq. S2)}$$

See *Materials and Methods* and *Table 1* for details. The gradient for inter-dimer longitudinal bond was written analogously to the gradient for lateral bond.

Appendix B. Determining parameters of MT dynamic instability from theoretical data and other model analyses

The output of numerical calculations, i.e. the coordinates and angles of tubulin monomers as a function of time, were analyzed using custom-written MATLAB programs (2012b, MathWorks). MT length at each time was defined as the average z-coordinate of the most distant dimers in each protofilaments. The onset of MT growth was defined as the time point when MT length increased by at least 20 nm. Introducing this rule was necessary for a consistent comparison between MT starting from a blunt "seed" and MT re-growing from the "seed" after a previous cycle of polymerization-depolymerization. Often, MTs depolymerized incompletely, leaving the residual protofilament curls less than 20 nm in length, so the growth was assumed to take place when MT length exceeded the 20 nm threshold.

Polymerization rate was calculated as a slope of the length vs. time dependency smoothed by applying 80 ms moving average. The depolymerization phase was defined as the time period during which the MT length decreased by at least 32 nm (8 monomer layers). Thus, fluctuations in the MT length less than 8 monomer layers were attributed to the variability in MT length during its growth, rather than to depolymerization and rescue. MT catastrophe time was defined using an automated algorithm written in MATLAB (Fig. S2B inset). MT rescues were infrequent, consistent with a rare occurrence of these events in vitro.

Fluctuations in MT length were calculated as the length increments for a leading protofilament during simulated MT growth with 0.1 s sampling intervals, as in experiments with low force in (55) (Fig. S1C). EB comet profiles were simulated via a convolution of the calculated GTP-tubulin dimer distribution with the Gaussian point-spread function corresponding to 512 nm emission wavelength of GFP (61, 62). EB comet size was calculated as the characteristic length of the resulting exponentially decaying profile. A good match to data in (63) was obtained for $K_{hydrol,} = 0.11\ s^{-1}$, same value as used elsewhere in the paper for model comparison with experimental data; other model parameters were as in Table 1 (Fig. S1D).

Appendix C. Normalizing results of the calculations with accelerated rate of GTP hydrolysis

The catastrophe frequency in our model is proportional to K_{hydrol} in the range from 3 to 11 s^{-1} (Fig. 3A), implying that modeling results obtained with high hydrolysis rates can be used to study MT catastrophes at normal hydrolysis rate 0.1 - 0.5 s^{-1} (7, 45), which are not computationally accessible with current tools. When the linear fit in Fig. 3A is extrapolated to this hydrolysis rate range, the predicted catastrophe frequency is $(3 - 15)\cdot10^{-3}\ s^{-1}$, similar to the experimental range (24, 25, 31, 40, 64, 65). Differences in the reported catastrophe frequencies often reflect different experimental conditions, such as buffer composition or temperature. Unless stated otherwise, theoretical results reported here have been scaled to represent $K_{hydrol,} = 0.11\ s^{-1}$, because this value provides the best match to experimental catastrophe frequency $(3 - 3.5)\cdot10^{-3}\ s^{-1}$ reported in (24), where MT aging was studied in details. Specifically, data obtained in our model with $K_{hydrol} = 9\ s^{-1}$ were normalized by "slowing down" the modeling time by a factor of 82 (ratio of the accelerated to experimental hydrolysis rate constants) prior to plotting (Fig. 3 panels B-F, Fig. 4 panel B catastrophe frequency, Fig. 4 panels C and D, Fig. 7 panel C). When such scaling is applied to the lifetime distributions calculated using different K_{hydrol} value (Fig. S3A), the normalized distributions are similar, justifying this approach. To further test this scaling procedure we also calculated three additional model outputs: size of the cap (number of GTP subunits), characteristic time to achieve a steady state for the cap size and the frequency of encountering different number of protofilament curls. All these dependencies are described by linear functions (Fig. S3B,C; note that the reciprocals of the GTP-cap size

and characteristic time are plotted), strongly suggesting that the composition and conformation of the MT tip are scalable at different hydrolysis rate. These results also imply that the mechanisms of MT catastrophe at different hydrolysis rates are fundamentally similar.

Appendix D. Comparison of modeling parameters used in current work and in the mechanochemical models

The mechanochemical model based on the original approach developed by VanBuren et al. (16) has previously been used to predict the unbounded increase in MT tip tapering during MT growth (41), while MT tapering in our model reaches a steady-state quickly. To try to understand why these models behave differently we compared the values of model parameters, which were used to make these predictions. Consistent with the results from MT nanoindentations in silico (49), our model uses relatively strong tubulin-tubulin bonds: the lateral and longitudinal bond energies are 9.1 and 15.5 k_BT, respectively (Table 1). The mechanochemical models in (16, 41, 56) employ somewhat similar energy bond ratios, such that the lateral bond is weaker than the longitudinal one, however, these energies correspond to relatively weak interactions: 3.2 - 5.7 and 6.8 - 9.5 k_BT for the lateral and longitudinal bonds, respectively. The direct comparison between energy values in these and our model is difficult, however, because these models differ in the overall shape of tubulin energy potentials. Here, and in our previous models (17, 38, 39), we use energy potential with a well and an activation barrier (Fig. S1A), consistent with protein-protein interaction studies (66), while the energy profile in mechanochemical model is a potential well (e.g. Fig. 1B in (16)).

Other difference between two modeling approaches is our use of a much slower rate constant for tubulin addition: 8.3 $\mu M^{-1}s^{-1}$ vs. 58-65 $\mu M^{-1}s^{-1}$ per MT in more recent versions of the mechanochemical model (41, 56). Importantly, the values for this constant and the energy parameters are not user-defined, but they are determined from model calibrations, i.e. fitting the model to obtain a match to specific experimental dependencies. As described in Materials and Methods section *Choice of Model Parameters and Model Calibration*, in our model the value for $k_{on,MT,}$ is determined from the MT polymerization rate dependency in Fig. 2B. The 8.3 $\mu M^{-1}s^{-1}$ value we obtain is close to some experimental reports, e.g. (25). When the value of $k_{on,MT}$ is increased in our model without changing other parameters, the rate of MT growth increases proportionally, as expected, and it no longer matches the experimental range. Since our model does not permit a direct control over the dissociation constant k_{off}, the increase in MT polymerization rate due to a faster $k_{on,MT}$ can be compensated only indirectly, e.g. by weakening the energy of tubulin-tubulin bonds. Incorporating in our model a faster $k_{on,MT}$ together with weaker bond energies recovers the physiological MT polymerization rate at 7-8 µM soluble tubulin, but it leads to a steeper slope than in experiment (Fig. S1B). More significantly, with this set of model parameters, the rate of MT shortening in our model is predicted to be 12,000 µm/min. It appears that such unrealistically fast MT disassembly prediction is a direct consequence of a high flexural rigidity of protofilament bending in our model (300 $k_BT\ rad^{-2}$, Table 1), while the mechanochemical models use only 50-60 $k_BT\ rad^{-2}$ (16, 41). Although we have not done the exhaustive analysis of model predictions for different combinations of parameter values, we believe that it should be possible to match the experimental dependency in Fig. 2B and the physiological MT depolymerization rate within the frame of our model using weaker protofilament rigidity and tubulin-tubulin bond energies, and a faster on-rate, similar to the parameter sets employed by the mechanochemical models. However, when protofilament rigidity is reduced, our model can no longer match the results of experiments on force generation by depolymerizing MTs (33, 34). Clearly, the requirement for large protofilament rigidity is not ungrounded, because generation of the power strokes by bending protofilaments is the only known mechanism to explain large forces developed by

depolymerizing MTs in vitro (35, 49). It is a unique feature of our model, however, that it can match multiple MT experiments with one set of model parameters, which severely constrains their possible values. Indeed, values of most parameters in our model cannot be changed significantly without losing the match to at least one of the key experiments, preventing us from using parameter values that work well in other models, in which the set of matched experiments was not as broad. To conclude, our limited analysis indicates that the unbounded increase in MT end tapering, as seen with the mechanochemical model (41), could potentially result from weak tubulin-tubulin interaction energies used in that model. Without strong bonding between tubulins, protofilaments can elongate semi-independently from each other, accompanied by a linear increase in the variance of their lengths. This hypothesis, however, needs further analysis of the behavior of different models and their continued experiment-based verification.

Appendix E. Fine structure of the MT tip predicted by the current model and in vitro

Different electron microscopy (EM) techniques have previously been used to examine the ends of MTs grown in vitro, but these results are controversial. In a transmission EM study of 29 MTs (41) the tips showed a narrow variation in tip extension length, with the mean increasing linearly from ~20 to 90 nm as the MT length increased from ~1 to 4 μm (Fig. 3B in (41)). Although our predicted theoretical extension length for this tubulin concentration (60-75 nm, Fig. 5C) lies within the range reported in (41), in the model the length of tip extensions increases soon after the start of polymerization and it remains constant for all MTs longer than ~ 150 nm. In a cryo-EM study in (31), a total of 2,910 MTs were examined for 3 tubulin concentrations and at least 3 time points (Table IV in (31)). To compare these results with predictions of our model we digitized data in Figs. 8 and 9 in (31) using GetData Graph Digitizer program and built cumulative distribution functions (Fig. S5 graphs). Two-sample Kolmogorov-Smirnov test was used to carry out pairwise comparisons of distributions at different time points for each tubulin concentration (Fig. S5 tables). Normalized Kolmogorov-Smirnov statistics was calculated with parameter D:

$$D = \sqrt{\frac{N_2 N_1}{N_1 + N_2}} \max|CDF_1(x) - CDF_2(x)| \qquad \text{(Eq. S3)}$$

Here, N_1 and N_2, sample sizes for each distribution, were taken from Table IV in (31).

This analysis revealed that out of 12 pairwise comparisons of the distributions of MT tip extensions documented in (31), five pairs showed no statistically significant differences at different MT lifetimes (Fig. S5). Seven pairs were significantly different but they did not form a specific trend: three pairs had a decrease in tapering with increasing MT age and four pairs had an increase in tapering. The lack of a reliable increase in the extension length in the cryo-EM study (31) is in tune with our model's prediction. Also, as in our model, the extension length was reported to increase with increasing tubulin concentration (31), although in the model the tip extension was less sensitive to tubulin concentration (Fig. 5C). We note that more recent experiments by this group (67) reported that growing MT tips had much shorter extensions at high tubulin concentrations (median values ~20 nm for 45 μM tubulin and ~80 nm for 90 μM tubulin), suggesting that the dependence of MT tip extension on tubulin concentration in vitro is not as strong as reported previously.

Fine structure of the MT tip has also been analyzed in previous experimental studies by quantifying standard deviation of the MT tip images obtained with fluorescence microscopy (41, 56, 58, 61). These studies have concluded that protofilament protrusions increase with increasing tubulin concentration, in agreement with results of the EM study in (31) and of the current model. Coombes et al. (41) additionally

report that SDs of the MT tips increase with time (150-300 nm at 12 μM tubulin); this increase was suggested to reflect a progressive tip tapering during MT growth. In contrast, a more recent fluorescent microscopy study (58) measured the significantly lower average SD values for the growing MT tips (<145 nm at 11-38 μM tubulin), consistent with our model's predictions. This experimental study also estimates that fluorescence-based microscopy cannot resolve reliably the MT tapers shorter than 180 nm, so our predicted MT tip protrusions might be below a detection limit for this technique.

Appendix F. Simplified stochastic model of MT evolution and catastrophe

The system (MT) was assumed to have several distinct configurations or states $\{S_i\}$, characterized by specific molecular features (black dots at the MT tip in Fig. 9A). Initially, the MT was in state S_0, and transitions between all subsequent states occurred with characteristic times t_f and t_b for forward and backward transitions, respectively,

$$S_o \underset{t_b}{\overset{t_f}{\rightleftarrows}} S_1 \underset{t_b}{\overset{t_f}{\rightleftarrows}} \ldots \xrightarrow{t_f} S_N \qquad \text{(Eq. S4)}$$

For a given time step *dt*, the probability of a transition *P* was calculated as

$$P_{f/b} = 1 - \exp(-\, dt \,/\, t_{f/b}) \qquad \text{(Eq. S5)}$$

Here, $t_{f/b}$ is the ratio of the forward to backward time constants. The script for calculations was written in MATLAB 2012; time step *dt* was selected at least 10-fold shorter than the smallest time constant. Using Eq. S5, 1000 simulations were carried out to determine MT lifetime, i.e. the total time for the system to transit from initial S_0 state to final S_N state. Multiple parameter sets (N, t_f, t_b) can provide a good match between this model and the experimental bell-shaped distribution of the MT lifetime (Fig. 9B). Importantly, the larger number of states N enables the faster transitions (i.e. short-lived evens) (Fig. 9C). Thus, this model illustrates that in complex stochastic systems, the time to reach the last "catastrophe" state (state with n=12 in Fig. 9D) can be two orders of magnitude slower than the characteristic time of individual transitions. MT aging can, therefore, represent a property of a complex stochastic system (MT tip) to approach gradually the steady state for the occurrence of the large number of short-lived features that promote MT catastrophe (black dots at the MT tip in state (N-1) in Fig. 9A). Unlike the permanent "hits" (model with N=3, Fig. 9B), in models with large Ns the short-lived "defects" are repairable, i.e. they arise and disappear continuously, so the MT aging represents the kinetics of the increase in probability to encounter these infrequent features, rather than their continuous accumulation.

Supplemental References

61. Demchouk, A.O., M.K. Gardner, and D.J. Odde. 2011. Microtubule Tip Tracking and Tip Structures at the Nanometer Scale Using Digital Fluorescence Microscopy. Cell. Mol. Bioeng. 4: 192–204.

62. Zhang, B., J. Zerubia, and J.-C. Olivo-Marin. 2007. Gaussian approximations of fluorescence microscope point-spread function models. Appl. Opt. 46: 1819–1829.

63. Bieling, P., L. Laan, H. Schek, E.L. Munteanu, L. Sandblad, M. Dogterom, D. Brunner, and T. Surrey. 2007. Reconstitution of a microtubule plus-end tracking system in vitro. Nature. 450: 1100–1105.

64. Fygenson, D.K., E. Braun, and A. Libchaber. 1994. Phase diagram of microtubules. Phys. Rev. E. 50: 1579–1588.

65. Janson, M.E., M.E. de Dood, and M. Dogterom. 2003. Dynamic instability of microtubules is regulated by force. J. Cell Biol. 161: 1029–1034.

66. Laue, T., and B. Demeler. 2011. A postreductionist framework for protein biochemistry. Nat. Chem. Biol. 7: 331–334.

67. Vitre, B., F.M. Coquelle, C. Heichette, C. Garnier, D. Chrétien, and I. Arnal. 2008. EB1 regulates microtubule dynamics and tubulin sheet closure in vitro. Nat. Cell Biol. 10: 415–421.

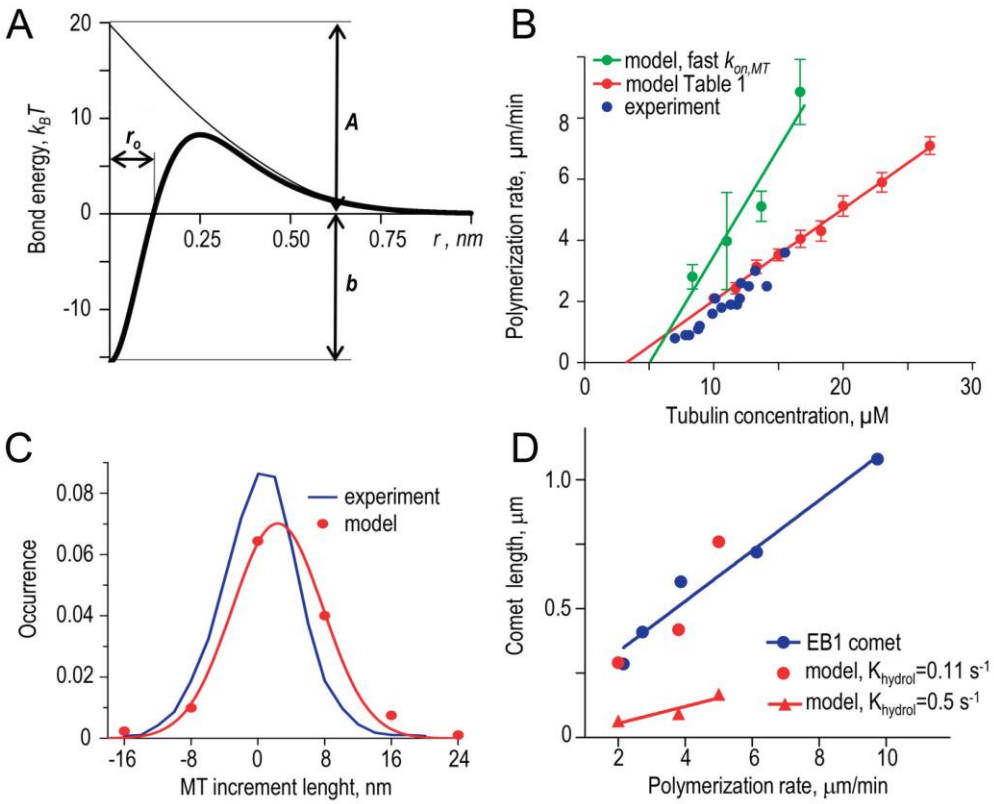

Figure S1. Quantitative analyses of the growing MT end

A. Potential energy profile for tubulin-tubulin interactions (lateral bonds and longitudinal inter-dimer bonds) used in this model. Exponent (thin line) is the first term in Eq. 1; *r* is distance between interaction points. See Fig. 1C and Table 1 for details.

B. Dependence of the MT growth rate on soluble tubulin concentration. Experimental data are from (25). Predictions of the current model with parameters listed in Table 1 are in red (same graph as in Fig. 2B). Green dots are predictions of the current model with parameters listed in Table 1 except the following changes: $k_{on,MT}$ = 58 µM s^{-1}, b_{lat} = 4.7 k_BT, b_{inter} = 9.5 k_BT, A_{lat} = 4.3 k_BT, A_{inter} = 4.8 k_BT. Each theoretical data point is the mean of 8-16 repeats, bars are SDs. Lines are liner fits to theoretical data.

C. Normalized histograms of increment lengths during MT polymerization. Experimental distribution is based on data in Fig. 5 in (55). Red dots are predictions of the current model for 6 µM tubulin (N=960) with parameters listed in Table 1, red line is Gaussian fitting. SDs for MT length increments are 4.5 and 5.4 nm for experiment and model, respectively.

D. Size of the "comets" at the growing MT ends as a function of MT polymerization rate. Experimental data are for the comet tail lengths formed by EB1 homolog Mal3 (data from Fig. 2c in (63)). Model predictions are for parameter values in Table 1 and two different GTP hydrolysis rates.

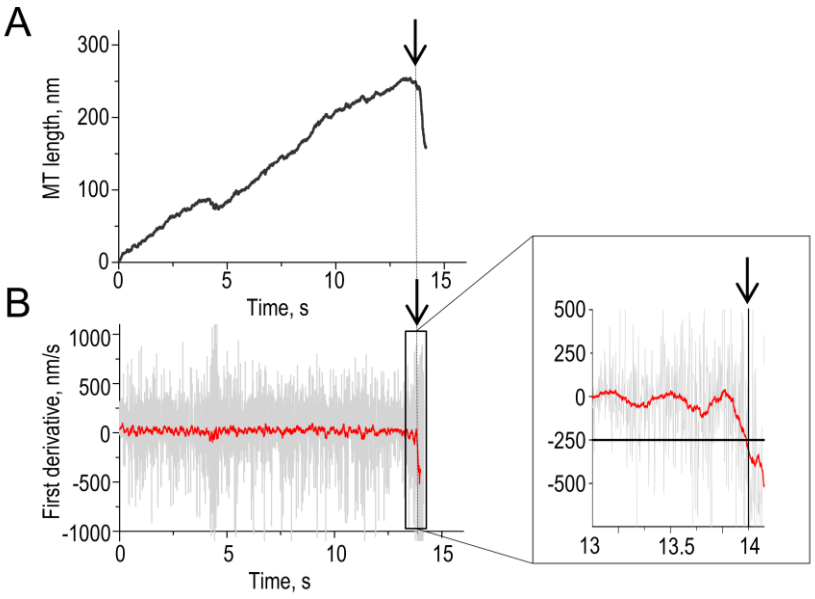

Figure S2. Algorithm to determine the time of MT catastrophe.

A. Example simulation in which MT length is plotted vs. model time (with no normalization). Data were sampled with 2 ms interval, shown after applying 80 ms moving average. Arrow points to catastrophe. Soluble tubulin concentration 10 µM, K_{hydrol} = 9 s^{-1}.

B. First derivative of the curve in panel A was calculated prior to (in grey) or after (in red) smoothing with a moving average. Inset shows enlargement of the last ~ 1 s of the simulation, revealing the onset of rapid shortening. The catastrophe time (arrow) was defined as the time point when the rate of depolymerization reached -250 nm/s (15 µm/min, horizontal black line in inset graph) and shortening continued for at least 8 monomer layers.

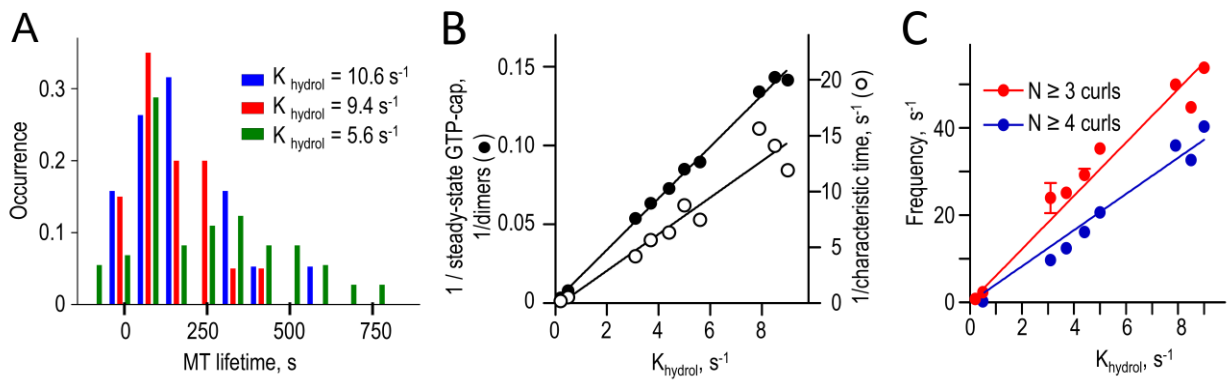

Figure S3. Scaling of model outputs calculated with different GTP hydrolysis rate.

A. Normalized distributions of MT lifetimes for different hydrolysis constants. Histograms are based on the results of N = 73, 19 and 20 simulations with K_{hydrol} = 5.6, 9.4 and 10.6 s^{-1}, respectively. Lifetimes obtained in these simulations were normalized using multiplication factor K_{hydrol}/ 0.11 s^{-1} before plotting.
B. Steady-state GTP-cap size and the corresponding characteristic time (reciprocal values are plotted) as a function of the GTP hydrolysis rate based on at least 32 simulations for each rate. Lines are linear fits for calculations with accelerated K_{hydrol} (> 3 s^{-1}). Unlike with catastrophe frequency, the size of the cap and its characteristic time can also be calculated with the realistic hydrolysis rate (shown for 0.5 s^{-1}). Importantly, the direct calculations with this slow rate and the linear extrapolation for accelerated hydrolysis rate lead to highly similar values, validating the scaling approach.
C. Frequency to encounter a given number of protofilament curls at the MT end growing at steady state as a function of the GTP hydrolysis rate. See legend to panel B for more details.

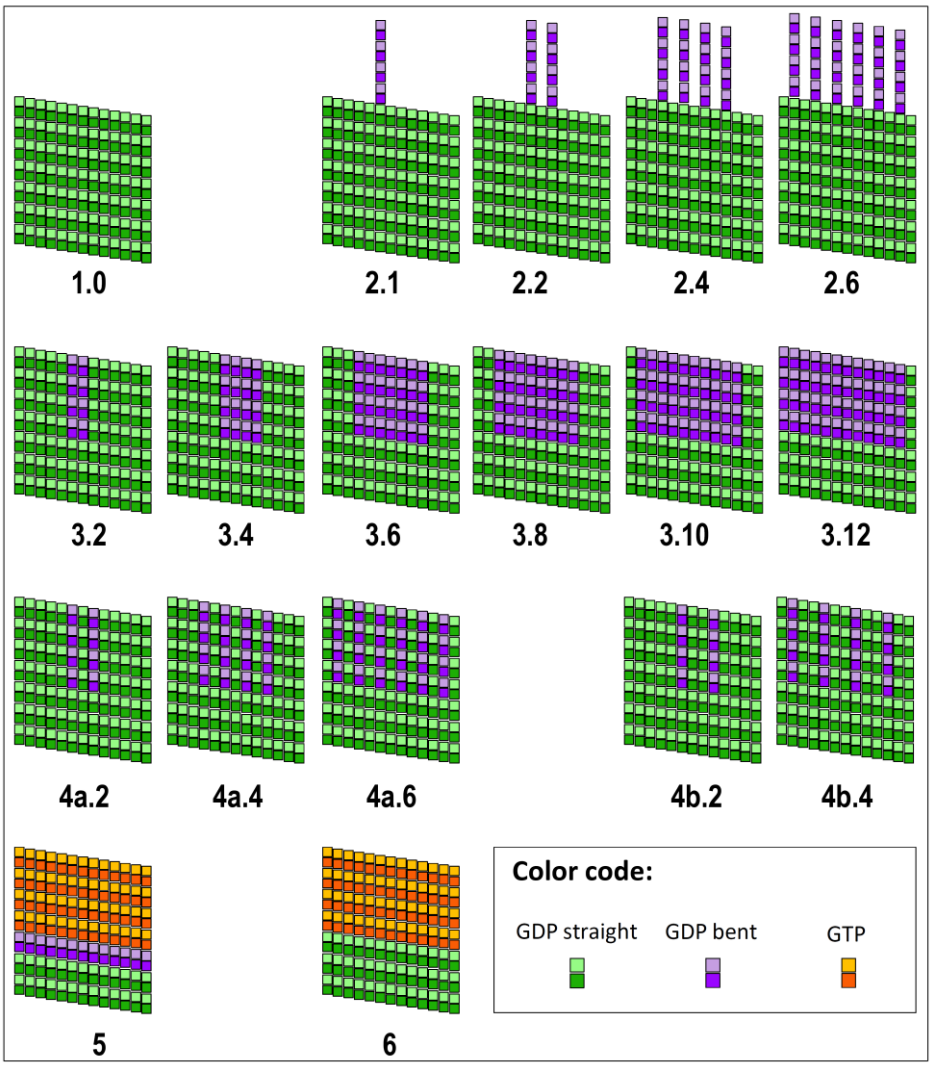

Figure S4. Diagrams of MT tip configurations used for calculations reported in Table 2.

Selected tip structures (flat representation), which were used as starting configurations for calculations with 10 μM tubulin. Different shades show α and β tubulin monomers. Leftmost protofilament in each diagram adheres to the rightmost protofilament to close into helical MT cylinder. Note that configurations in groups 3 and 4 have some straight protofilaments that lack lateral bonds with at least one neighbor, while in group 2 all straight protofilaments have lateral bonds, explaining the dramatically different stabilities of these configuration groups.

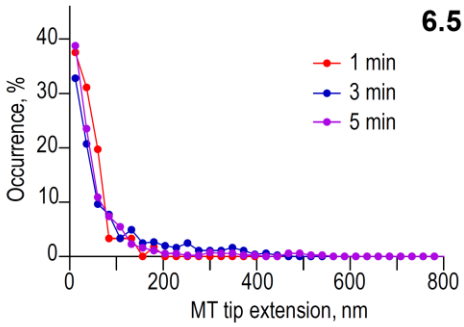

Pair for comparison	D	significance level (α)
1 min vs 3 min	1.82	** (p<0.005)
1 min vs 5 min	1.10	NS (p> 0.1)
3 min vs 5 min	1.57	* (p<0.05)

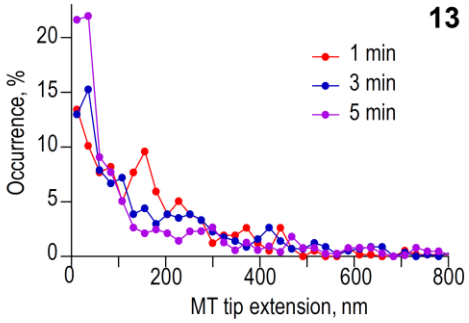

Pair for comparison	D	significance level (α)
1 min vs 3 min	1.03	NS (p> 0.1)
1 min vs 5 min	2.26	*** (p<0.001)
3 min vs 5 min	2.64	*** (p<0.001)

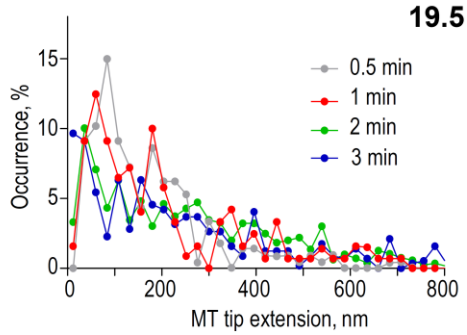

Pair for comparison	D	significance level (α)
0.5 min vs 1 min	1.18	NS (p> 0.1)
0.5 min vs 2 min	3.18	*** (p<0.001)
0.5 min vs 3 min	2.44	*** (p<0.001)
1 min vs 2 min	1.86	** (p<0.005)
1 min vs 3 min	1.35	NS (p> 0.1)
2 min vs 3 min	1.05	NS (p> 0.1)

Figure S5. Statistical analysis of MT tip extension distributions reported in (31).

Histogram distributions of the extension lengths observed at the ends of MTs that polymerized for indicated time and at indicated soluble tubulin concentration. These graphs were built by digitizing the corresponding distribution reported in Figs. 8 and 9 in (31). D was calculated with Eq. S3 (Appendix E); $D < 1.36$ means no significant difference ($p > 0.05$). Parameter α is a significance level at which null hypothesis of distributions' equality is rejected. NS – not significant.